

The square lattice Ising model on the rectangle

II: Finite-size scaling limit

Alfred Hucht

Faculty for Physics, University of Duisburg-Essen, 47058 Duisburg, Germany

Abstract

Based on the results published recently [1], the universal finite-size contributions to the free energy of the square lattice Ising model on the $L \times M$ rectangle, with open boundary conditions in both directions, are calculated exactly in the finite-size scaling limit $L, M \rightarrow \infty$, $T \rightarrow T_c$, with fixed temperature scaling variable $x \propto (T/T_c - 1)M$ and fixed aspect ratio $\rho \propto L/M$. We derive exponentially fast converging series for the related Casimir potential and Casimir force scaling functions. At the critical point $T = T_c$ we confirm predictions from conformal field theory [2, 3]. The presence of corners and the related corner free energy has dramatic impact on the Casimir scaling functions and leads to a logarithmic divergence of the Casimir potential scaling function at criticality.

CONTENTS

I. Introduction	3
II. Finite-size scaling theory	6
III. Scaling functions for the considered geometry	8
IV. Finite-size scaling limit of the strip residual partition function	10
A. The characteristic polynomial	10
B. Contour integration	13
C. Construction of counting polynomial $R(\Phi)$	14
D. Calculation of the integrals	15
E. Representation of the partition function scaling function $\Sigma(x, \rho)$	16
V. Results	18
A. Results at $x = 0$	18
B. Results for general x and ρ	21
C. The Casimir potential scaling function $\Theta(x, \rho)$	21
D. The Casimir force scaling function $\vartheta(x, \rho)$	24
VI. Scaling limit of effective spin model	26
VII. Conclusions	27
Acknowledgments	27
A. Series expansion for zeroes Φ_μ	27
B. Expansion of q -products around $q = 1$	28
References	29
References	29

I. INTRODUCTION

In the first part of this work [1], denoted I in the following, we computed the partition function Z of the two-dimensional Ising model on the $L \times M$ rectangle with open boundary conditions in both directions and with anisotropic reduced couplings K^{\leftrightarrow} and K^{\updownarrow} in horizontal and vertical direction, in units of $k_B T$ with Boltzmann constant k_B , at arbitrary temperatures below and above the critical point. This second part is devoted to the finite-size scaling (FSS) behavior near criticality.

We first recall the main results of part I in terms of the size dependent reduced free energy $F(L, M) = -\log Z$. From (I.87) we get the total free energy of the considered model,

$$\begin{aligned}
 F(L, M) = & \underbrace{-\frac{L}{2} \left[M \log \left(\frac{2}{-z_-} \right) + \sum_{\mu=1}^M \hat{\gamma}_\mu \right]}_{L f_{b,s}(M)} \\
 & - \underbrace{\frac{1}{2} \log \left[\left(\frac{2}{t_- z_-} \right)^{\frac{M^2}{2}} d_{\mathbf{o},\mathbf{e}}^2 \prod_{\mu=1}^M \frac{(t_+ z_+ - \hat{\lambda}_{\mu,+})^2 - t_-^2 z_-^2}{M \hat{\lambda}_{\mu,-}^2 + z_+ \hat{\lambda}_{\mu,+} - t_+} \frac{z \hat{\lambda}_{\mu,-}}{v_\mu} \right]}_{F_{s,c}(M)} \\
 & - \underbrace{\log \det(\mathbf{1} + \mathbf{Y})}_{F_{\text{strip}}^{\text{res}}(L, M)}, \tag{1}
 \end{aligned}$$

where $\hat{\lambda}_\mu = e^{\hat{\gamma}_\mu} > 1$ are the M dominant eigenvalues of the $2M \times 2M$ transfer matrix \mathcal{T}_2 (I.27), given by the positive zeroes of the characteristic polynomial $P_M(\varphi)$ (I.45). Alternatively, $\hat{\lambda}_{\mu,+} = \cosh \hat{\gamma}_\mu$ are the M eigenvalues of \mathcal{T}_+ (I.30a). $z = \tanh K^{\leftrightarrow}$ and $t = \exp(-2K^{\updownarrow})$ parametrize the two couplings, and $a_\pm \equiv \frac{1}{2}(a \pm a^{-1})$ is a handy shortcut from (I.20). For a definition of the other quantities $d_{\mathbf{o},\mathbf{e}}$ (I.70b), v_μ (I.87a) and the $M/2 \times M/2$ residual matrix \mathbf{Y} (I.87b) the reader is referred to part I. In (1) we decomposed the leading term F_{strip} from (I.92) into two parts,

$$F_{\text{strip}}(L, M) = L f_{b,s}(M) + F_{s,c}(M), \tag{2}$$

one proportional to L with contributions from the bulk and from the two horizontal (\leftrightarrow) surfaces, and one with the remaining contributions from the two vertical (\updownarrow) surfaces and from the four corners, see figure 1. These terms have been analyzed in great detail by R. J. Baxter recently¹ [4].

¹ The couplings (z, t) are denoted (t^*, u^*) in [4], where $z^* = \frac{1-z}{1+z}$ is the dual of z .

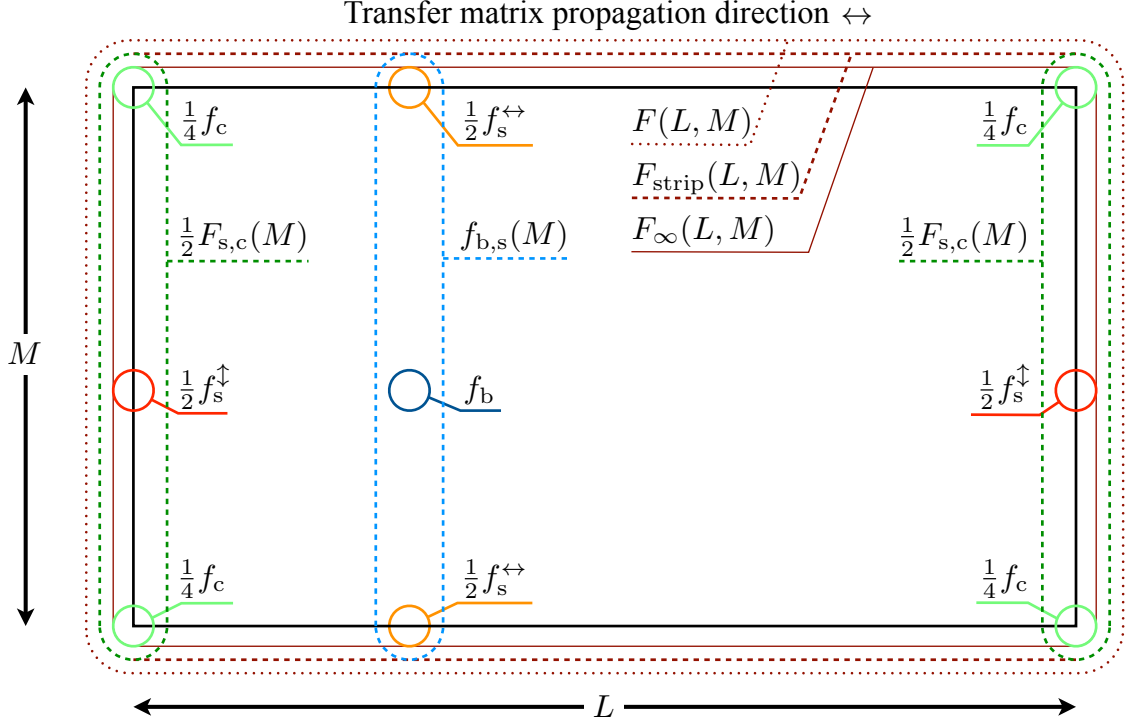


Figure 1. Sketch of the decomposition of the total free energy $F(L, M)$ (dotted line) into the different constituents. The black rectangle is the system, and the other solid lines denote infinite volume contributions solely dependent on temperature, while the dashed lines symbolize free energy parts containing residual finite-size contributions.

For a detailed discussion of the different free energy contributions we also recall the definition of the (total) residual free energy, or Casimir potential, F_∞^{res} (I.89), which is responsible for nontrivial finite-size effects such as the critical Casimir effect [5],

$$F_\infty^{\text{res}}(L, M) \equiv F(L, M) - F_\infty(L, M), \quad (3a)$$

where the infinite volume contribution F_∞ can be decomposed into bulk, surface and corner contributions according to (I.90)

$$F_\infty(L, M) \equiv LM f_b + L f_s^{\leftrightarrow} + M f_s^{\updownarrow} + f_c \quad (3b)$$

for our rectangular geometry. The bulk free energy per spin f_b , the surface free energies per surface spin pair f_s^δ , with direction $\delta \in \{\leftrightarrow, \updownarrow\}$, and the corner free energy f_c are defined in the thermodynamic limit $L, M \rightarrow \infty$ and do not depend on L or M . While f_b and f_s^δ are known since a long time from the seminal works of Onsager [6] and McCoy

& Wu [7], the corner free energy f_c below T_c was derived only recently by Baxter² [4], confirming a conjectured product formula by Vernier & Jacobsen [8]. The corresponding product formula for temperatures above T_c was given in (I.A7d). The logarithmic divergence $f_c \simeq \frac{1}{8} \log |1 - T/T_c| + \mathcal{O}(1)$ detailed in appendix B will lead to a considerable complication of the FSS analysis, as shown below.

Comparing (1) with (3), we first focus on the L dependent terms. The free energy per row $f_{b,s}$ is the dominant outcome of one application of the transfer matrix \mathcal{T}_2 . It can be further decomposed,

$$f_{b,s}(M) = M f_b + f_s^{\leftrightarrow} + f_{b,s}^{\text{res}}(M), \quad (4)$$

and contains a residual contribution at finite M that is equal to the leading large- L contribution to F_∞^{res} from (I.94),

$$f_{b,s}^{\text{res}}(M) \equiv \lim_{L \rightarrow \infty} L^{-1} F_\infty^{\text{res}}(L, M). \quad (5)$$

Inserting (4) into (1),

$$F(L, M) = L [M f_b + f_s^{\leftrightarrow} + f_{b,s}^{\text{res}}(M)] + F_{s,c}(M) + F_{\text{strip}}^{\text{res}}(L, M), \quad (6)$$

and matching with (3), we can eliminate the leading L -dependent terms and find three contributions to the total residual free energy (3a),

$$F_\infty^{\text{res}}(L, M) = L f_{b,s}^{\text{res}}(M) + F_{s,c}^{\text{res}}(M) + F_{\text{strip}}^{\text{res}}(L, M), \quad (7)$$

where we defined the residual surface-corner contribution

$$F_{s,c}^{\text{res}}(M) \equiv F_{s,c}(M) - [M f_s^\dagger + f_c], \quad (8)$$

which is independent of L . Equation (7) shows that the residual free energy can be decomposed very similar to (3).

We now turn to the critical Casimir force per area M , that is defined as L -derivative of the total residual free energy (3a),

$$\mathcal{F}(L, M) \equiv -\frac{1}{M} \frac{\partial}{\partial L} F_\infty^{\text{res}}(L, M), \quad (9)$$

² A constant term $-\log 2$ attributed to $f_c^<$ in [1, 4] stems from the broken symmetry below T_c and has to be moved from F_∞ to F_∞^{res} , see section V C.

and by (7) decomposes into two contributions,

$$\mathcal{F}(L, M) = \underbrace{-\frac{1}{M} f_{\text{b,s}}^{\text{res}}(M)}_{\mathcal{F}_{\text{b,s}}(M)} - \underbrace{\frac{1}{M} \frac{\partial}{\partial L} F_{\text{strip}}^{\text{res}}(L, M)}_{\mathcal{F}_{\text{strip}}(L, M)}, \quad (10)$$

where the first one $\mathcal{F}_{\text{b,s}}$ is already known from the stripe geometry $L/M \rightarrow \infty$. Note that the surface-corner contribution $F_{\text{s,c}}^{\text{res}}$ drops out in the L -derivative as expected [9, 10], which renders the analysis of the Casimir force \mathcal{F} simpler than the analysis of the Casimir potential F_{∞}^{res} .

With these definitions, we now summarize the FSS theory for the Casimir potential and Casimir force, and introduce the corresponding universal FSS functions.

II. FINITE-SIZE SCALING THEORY

In this chapter we will formulate the finite-size scaling theory for the residual free energy, or critical Casimir potential, as well as for the critical Casimir force per area in the general case of a d -dimensional weakly anisotropic system³ with size $V = L_{\leftrightarrow} L_{\updownarrow}^{d-1}$ and different couplings K^{\leftrightarrow} and K^{\updownarrow} . We use \leftrightarrow for the direction parallel to the force and \updownarrow for all other directions, and we rewrite $L_{\leftrightarrow} \equiv L$ and $L_{\updownarrow} \equiv M$ in this and in the following chapter. When we later apply this theory to our model, we will let the transfer matrix \mathcal{T} propagate parallel to the Casimir force, as the calculation of the force requires the derivative of the residual free energy with respect to L .

Near criticality, the anisotropic couplings K^{\leftrightarrow} and K^{\updownarrow} lead to weakly anisotropic critical behavior, characterized by a weakly anisotropic bulk correlation length⁴

$$\xi_{\infty}^{\delta}(\tau) \stackrel{\tau > 0}{\simeq} \xi_{+}^{\delta} \tau^{-\nu}, \quad (11)$$

where $\tau = T/T_c - 1$ denotes the reduced temperature, and ξ_{+}^{δ} denotes the correlation length amplitude in direction $\delta \in \{\leftrightarrow, \updownarrow\}$ above criticality. The correlation length exponent is $\nu = 1$ for the $2d$ Ising model. Finite-size scaling theory predicts that near the critical point $\tau \rightarrow 0$ and for $L_{\delta} \rightarrow \infty$ with fixed geometric aspect ratio $r = L_{\leftrightarrow}/L_{\updownarrow}$, the residual free energy F_{∞}^{res} (3a) only depends on the two length ratios $L_{\leftrightarrow}/\xi_{\infty}^{\leftrightarrow}(\tau)$ and $L_{\updownarrow}/\xi_{\infty}^{\updownarrow}(\tau)$ [11–13]. These two

³ For a discussion of weakly vs. strongly anisotropic critical behavior see, e. g., [11].

⁴ “ \simeq ” denoted “asymptotically equal”

ratios can be combined to a *reduced aspect ratio*

$$\rho \equiv \frac{L_{\leftrightarrow} \xi_+^\uparrow}{L_{\uparrow} \xi_+^{\leftrightarrow}} \stackrel{\tau \gtrsim 0}{\simeq} \frac{L_{\leftrightarrow} \xi_\infty^\uparrow(\tau)}{L_{\uparrow} \xi_\infty^{\leftrightarrow}(\tau)}, \quad (12a)$$

which does not depend on temperature and encodes both the system shape as well as the coupling anisotropy [11].

Approaching the critical point, the critical correlations are bounded by the smallest length ratio in the system. For the given geometry with arbitrary reduced aspect ratio ρ this leads to three different possible choices for the temperature scaling variable x [14, 15]: If $0 \leq \rho \lesssim 1$ ($1 \lesssim \rho \leq \infty$), the correlations are limited by L_{\leftrightarrow} (L_{\uparrow}), while for arbitrary finite aspect ratio $0 < \rho < \infty$ the geometric mean $L_o \equiv V^{1/d}$ can be used as relevant length, avoiding the preference for one direction δ . In all three cases, the temperature scaling variable is given by

$$x_\delta \equiv \tau \left(\frac{L_\delta}{\xi_+^\delta} \right)^{\frac{1}{\nu}} \stackrel{\tau \gtrsim 0}{\simeq} \left(\frac{L_\delta}{\xi_\infty^\delta(\tau)} \right)^{\frac{1}{\nu}}, \quad \delta \in \{\leftrightarrow, o, \uparrow\}, \quad (12b)$$

with geometric mean correlation length ξ_∞^o satisfying $\xi_\infty^o \equiv \xi_\infty^{\leftrightarrow} \xi_\infty^{\uparrow d-1}$, and the system is completely described by the two scaling variables x_δ and ρ in the FSS limit. The three variables x_δ obey the identity

$$x_{\leftrightarrow} \rho^{\frac{1}{d\nu} - \frac{1}{\nu}} = x_o = x_{\uparrow} \rho^{\frac{1}{d\nu}}. \quad (13)$$

Following Fisher & de Gennes [5], the residual free energy (3a) then fulfills the scaling *ansatz* [14, 15]

$$F_\infty^{\text{res}}(L_{\leftrightarrow}, L_{\uparrow}) \simeq \rho^{1-d} \Theta_{\leftrightarrow}(x_{\leftrightarrow}, \rho) = \Theta_o(x_o, \rho) = \rho \Theta_{\uparrow}(x_{\uparrow}, \rho), \quad (14)$$

with the universal Casimir potential scaling functions Θ_δ . Note that both $\Theta_{\leftrightarrow}(x_{\leftrightarrow}, \rho \rightarrow 0)$ and $\Theta_{\uparrow}(x_{\uparrow}, \rho \rightarrow \infty)$ are finite by construction, while $\Theta_o(x_o, \rho)$ diverges in both limits [14].

The Casimir force in \leftrightarrow direction per area L_{\uparrow}^{d-1} ,

$$\mathcal{F}(L_{\leftrightarrow}, L_{\uparrow}) \equiv -\frac{1}{L_{\uparrow}^{d-1}} \frac{\partial}{\partial L_{\leftrightarrow}} F_\infty^{\text{res}}(L_{\leftrightarrow}, L_{\uparrow}), \quad (15)$$

satisfies the finite-size scaling form

$$\mathcal{F}(L_{\leftrightarrow}, L_{\uparrow}) \simeq L_\delta^{-d} \vartheta_\delta(x_\delta, \rho) \quad (16)$$

for all three cases $\delta \in \{\leftrightarrow, o, \uparrow\}$, leading to the identities [14, 15]

$$\rho^{1-d} \vartheta_{\leftrightarrow}(x_{\leftrightarrow}, \rho) = \vartheta_o(x_o, \rho) = \rho \vartheta_{\uparrow}(x_{\uparrow}, \rho) \quad (17)$$

analogous to (14). We conclude with three scaling relations between Θ_δ and ϑ_δ [14, 15],

$$\vartheta_{\leftrightarrow}(x_{\leftrightarrow}, \rho) = - \left[1 - d + \frac{1}{\nu} \frac{x_{\leftrightarrow} \partial}{\partial x_{\leftrightarrow}} + \frac{\rho \partial}{\partial \rho} \right] \Theta_{\leftrightarrow}(x_{\leftrightarrow}, \rho) \quad (18a)$$

$$\vartheta_{\circ}(x_{\circ}, \rho) = - \left[\frac{1}{d\nu} \frac{x_{\circ} \partial}{\partial x_{\circ}} + \frac{\rho \partial}{\partial \rho} \right] \Theta_{\circ}(x_{\circ}, \rho) \quad (18b)$$

$$\vartheta_{\updownarrow}(x_{\updownarrow}, \rho) = - \left[1 + \frac{\rho \partial}{\partial \rho} \right] \Theta_{\updownarrow}(x_{\updownarrow}, \rho) = - \frac{\partial}{\partial \rho} [\rho \Theta_{\updownarrow}(x_{\updownarrow}, \rho)]. \quad (18c)$$

The FSS functions defined above are universal and only depend on the bulk and surface universality classes, the system shape and the boundary conditions. This universality was clearly demonstrated in [16], where the Casimir force scaling function $\vartheta(x, 0)$ of the XY universality class with Dirichlet boundary conditions showed quantitative agreement between experiments on liquid ^4He at the λ transition [17] and Monte Carlo simulations of the classical XY spin model on a simple cubic lattice [16], both in the thin film limit $\rho \rightarrow 0$. Subsequent theoretical studies [18, 19] as well as experiments on binary liquid mixtures [20–22] demonstrated the universal behavior within the framework of the Ising universality class, for an overview see, e.g., [23].

III. SCALING FUNCTIONS FOR THE CONSIDERED GEOMETRY

In a transfer matrix (TM) formulation as utilized in part I, the system can have arbitrary real length in propagation direction of the TM, while the other $d - 1$ lengths are fixed. Therefore, we identify \leftrightarrow with the propagation direction and use the scaling variable x_{\updownarrow} and the corresponding scaling functions $\Theta_{\updownarrow}(x_{\updownarrow}, \rho)$ and $\vartheta_{\updownarrow}(x_{\updownarrow}, \rho)$ for the description of the FSS behavior. In the following we will usually drop the index \updownarrow from the quantities $x_{\updownarrow} \equiv x$, $\Theta_{\updownarrow} \equiv \Theta$ and $\vartheta_{\updownarrow} \equiv \vartheta$ for simplicity.

Combining the residual free energy decomposition (7) with the scaling form (14) we now discuss the according decomposition of the scaling functions $\Theta(x, \rho)$ and $\vartheta(x, \rho)$ for the considered Ising model on the rectangle. Note that this discussion can be generalized to higher dimensions within a TM formulation. According to (7) and (14) we decompose Θ into three parts,

$$\Theta(x, \rho) = \Theta^{(\circ\circ)}(x) + \rho^{-1} \Theta_{\text{s,c}}(x) + \Psi(x, \rho), \quad (19)$$

where

$$\Theta^{(\circ\circ)}(x) \simeq L_{\updownarrow} f_{\text{b,s}}^{\text{res}}(L_{\updownarrow}) \quad (20)$$

is identified with the known Casimir potential scaling function for open boundary conditions in strip geometry $\rho \rightarrow \infty$ [24–26],

$$\Theta^{(\text{oo})}(x) \equiv -\frac{1}{2\pi} \int_0^\infty d\omega \log \left(1 + \frac{\sqrt{x^2 + \omega^2} - x}{\sqrt{x^2 + \omega^2} + x} e^{-2\sqrt{x^2 + \omega^2}} \right), \quad (21)$$

which becomes independent from the BCs in \leftrightarrow direction in this limit and can therefore be calculated from the known exact solution with periodic BCs in \leftrightarrow direction [15]. The second term in (19) contains the surface contributions from the \updownarrow edges as well as the corner contributions,

$$\Theta_{\text{s,c}}(x) \simeq F_{\text{s,c}}^{\text{res}}(L_\updownarrow), \quad (22)$$

is independent of ρ and will be discussed in chapter V C. Finally, the third term in (19) describes the strip residual free energy contribution, which fulfills

$$\rho \Psi(x, \rho) \equiv -\log \Sigma(x, \rho) \simeq F_{\text{strip}}^{\text{res}}(L_{\leftrightarrow}, L_\updownarrow), \quad (23)$$

where the scaling function Σ of the strip residual partition function (I.83) is given by

$$\Sigma(x, \rho) \simeq Z_{\text{strip}}^{\text{res}}(L_{\leftrightarrow}, L_\updownarrow) = e^{-F_{\text{strip}}^{\text{res}}(L_{\leftrightarrow}, L_\updownarrow)} \quad (24)$$

and will be computed in the next chapter. From the limit $\Psi(x, \rho \rightarrow \infty) \rightarrow 0$ [1] we get the expected result

$$\lim_{\rho \rightarrow \infty} \Theta(x, \rho) = \Theta^{(\text{oo})}(x). \quad (25)$$

According to (10), the total Casimir force scaling function (16) can be decomposed to

$$\vartheta(x, \rho) = -\Theta^{(\text{oo})}(x) + \psi(x, \rho), \quad (26)$$

where the strip Casimir force from (10),

$$\mathcal{F}_{\text{strip}}(L_{\leftrightarrow}, L_\updownarrow) \equiv -\frac{1}{L_\updownarrow^{d-1}} \frac{\partial}{\partial L_{\leftrightarrow}} F_{\text{strip}}^{\text{res}}(L_{\leftrightarrow}, L_\updownarrow), \quad (27)$$

contributes to the second term,

$$\psi(x, \rho) \equiv \frac{\partial}{\partial \rho} \log \Sigma(x, \rho) \simeq L_\updownarrow^d \mathcal{F}_{\text{strip}}(L_{\leftrightarrow}, L_\updownarrow), \quad (28)$$

while the other contribution

$$\Theta^{(\text{oo})}(x) \simeq -L_\updownarrow^d \mathcal{F}_{\text{b,s}}(L_\updownarrow) = L_\updownarrow \frac{\partial}{\partial L_{\leftrightarrow}} [L_{\leftrightarrow} f_{\text{b,s}}^{\text{res}}(L_\updownarrow)] = L_\updownarrow f_{\text{b,s}}^{\text{res}}(L_\updownarrow) \quad (29)$$

is again known (21) in our case. Note that the total Casimir force scaling function (26) could also have been obtained using the scaling relation (18c). In the following, we will first calculate the FSS function $\Sigma(x, \rho)$ and determine the Casimir force scaling function $\vartheta(x, \rho)$.

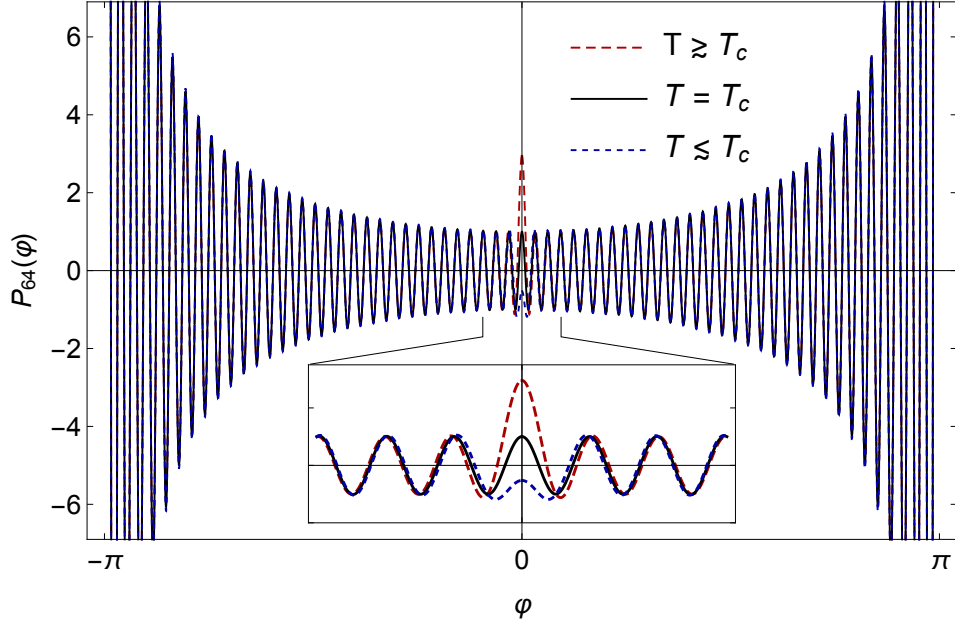


Figure 2. Characteristic polynomial $P_M(\varphi)$, Eq. (I.45), for $M = 64$ and three different temperatures above, at, and below T_c . The polynomials differ only around $\varphi = 0$, see inset.

IV. FINITE-SIZE SCALING LIMIT OF THE STRIP RESIDUAL PARTITION FUNCTION

A. The characteristic polynomial

We now turn back to the $2d$ Ising model on the $L \times M$ rectangle discussed in I and revert the variables L_{\leftrightarrow} and L_{\updownarrow} back to $L \equiv L_{\leftrightarrow}$ and $M \equiv L_{\updownarrow}$. We are allowed to assume isotropic couplings $t^* = z$ in the FSS limit in order to keep things simple, as near criticality a coupling anisotropy $K^{\leftrightarrow} \neq K^{\updownarrow}$ can be compensated by a scale transformation of the real variable $L \mapsto L\xi_+^{\updownarrow}/\xi_+^{\leftrightarrow}$ in conjunction with $K^{\leftrightarrow} \mapsto K^{\updownarrow}$, without changing the generalized aspect ratio ρ [11]. Then, the critical point is at $z = z_c \equiv \sqrt{2} - 1$, and we can use $\tau = 1 - z/z_c$ for the reduced temperature, with corresponding isotropic correlation length amplitude $\xi_+ = 1/2$. The resulting FSS variables x and ρ from (12) in terms of the relevant length M become

$$x = 2M \left(1 - \frac{z}{z_c}\right), \quad \rho = \frac{L}{M}. \quad (30)$$

We now perform the FSS limit of the results from I by replacing all quantities with the M -dependent scaling forms and then performing the limit $M \rightarrow \infty$ with fixed x and ρ . As the strip residual partition function $Z_{\text{strip}}^{\text{res}}$ is convergent in this limit, we do not encounter

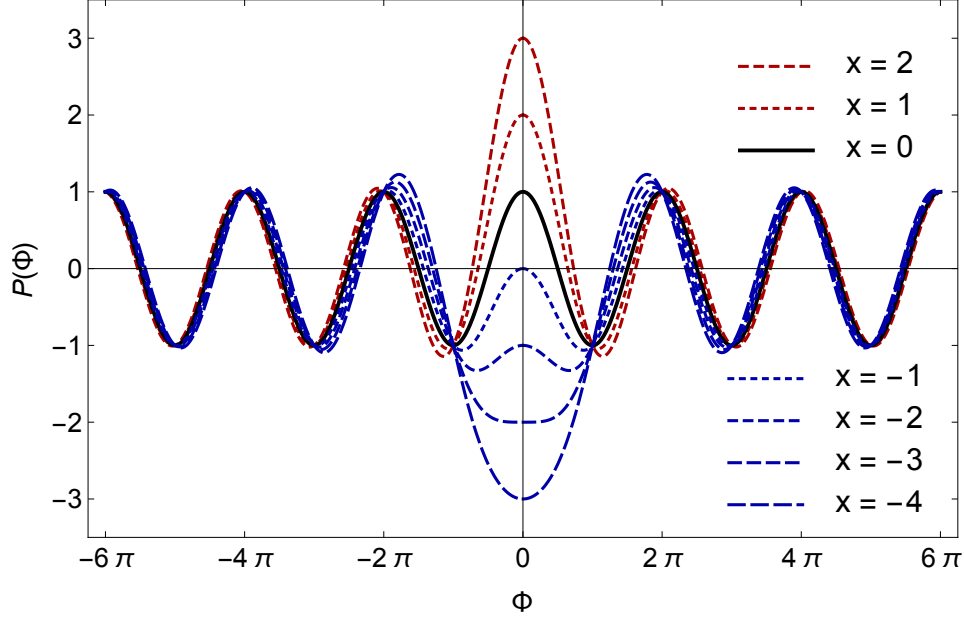


Figure 3. Universal characteristic polynomial $P(\Phi)$, Eq. (33), for different scaled temperatures x in the finite-size scaling limit. The first zero is doubly degenerate at $x = -1$ and becomes imaginary below.

regularization problems as in the case of the edge contribution $F_{s,c}$ discussed later. We will use the tilde $\tilde{\cdot}$ for quantities in the FSS limit and capitals for scaling variables.

Therefore, we replace the temperature variable z and the length L according to

$$z \mapsto z_c \left(1 - \frac{x}{2M}\right), \quad L \mapsto \rho M, \quad (31)$$

and first turn to the characteristic polynomial $P_M(\varphi)$ (I.45). For large M the relevant scaling contributions are obtained by a rescaling of the angle variable $\hat{\varphi}$ (I.86) according to

$$\hat{\varphi} \mapsto \frac{\Phi}{M}, \quad (32)$$

which immediately leads to the remarkably simple universal FSS form of the characteristic polynomial (I.45),

$$P(\Phi) \equiv \cos \Phi + \frac{x}{\Phi} \sin \Phi, \quad (33)$$

with infinitely many zeroes Φ_μ , $\mu \in \mathbb{N}$. All zeroes Φ_μ are real and positive except Φ_1 , which is zero for $x = -1$ and becomes imaginary for $x < -1$, see figure 3 and table I.

Comparing $P(\Phi)$ with $P_M(\varphi)$ of a finite system as shown in figure 2, we notice the following: while for small $|\varphi| \lesssim \pi/2$ both curves become more and more similar for large M ,

x	Φ_1	Φ_2	Φ_3	Φ_4
-4	3.997302692 i	3.916435368	7.355927023	10.63585142
-3	2.984704585 i	4.078149765	7.472192660	10.72277106
-2	1.915008048 i	4.274782271	7.596546020	10.81267333
-1	0	4.493409458	7.725251837	10.90412166
0	$\pi/2$	$3\pi/2$	$5\pi/2$	$7\pi/2$
1	2.028757838	4.913180439	7.978665712	11.08553841
2	2.288929728	5.086985094	8.096163603	11.17270587
3	2.455643863	5.232938454	8.204531363	11.25604301
4	2.570431560	5.354031841	8.302929183	11.33482558

Table I. Location of the first few zeroes of $P(\Phi)$, (33), for $\mu = 1, \dots, 4$ and several values of x .

the deviations for $|\varphi| > \pi/2$ stem from the lattice dispersion encoded in $P_M(\varphi)$, which is different from the continuum dispersion of $P(\Phi)$. We will see below that a careful regularization of the resulting infinite products is necessary in order to overcome the UV singularities emerging in the FSS limit.

The scaling limit of the eigenvalues $\hat{\lambda}$, expressed through the Onsager- $\hat{\gamma}$, is determined from the isotropic version of (I.43),

$$\cos \hat{\varphi} = z_+^* z_+ - \cosh \hat{\gamma}, \quad (34)$$

under the rescaling

$$\hat{\gamma} \mapsto \frac{\Gamma}{M}, \quad \hat{\lambda}^{-L} = e^{-L\hat{\gamma}} \mapsto e^{-\rho\Gamma}, \quad (35)$$

to be

$$\Gamma = \sqrt{x^2 + \Phi^2}. \quad (36)$$

At the zeroes Φ_μ we find the simple relation

$$\Phi_\mu \cot \Phi_\mu = \sigma_\mu \Gamma_\mu \cos \Phi_\mu = -x, \quad (37)$$

with parity (I.76)

$$\sigma_\mu \equiv (-1)^{\mu-1}. \quad (38)$$

The two remaining quantities entering the residual matrix \mathbf{Y} (I.87b), p_μ and v_μ from (I.74) and (I.87a), are calculated in the next section.

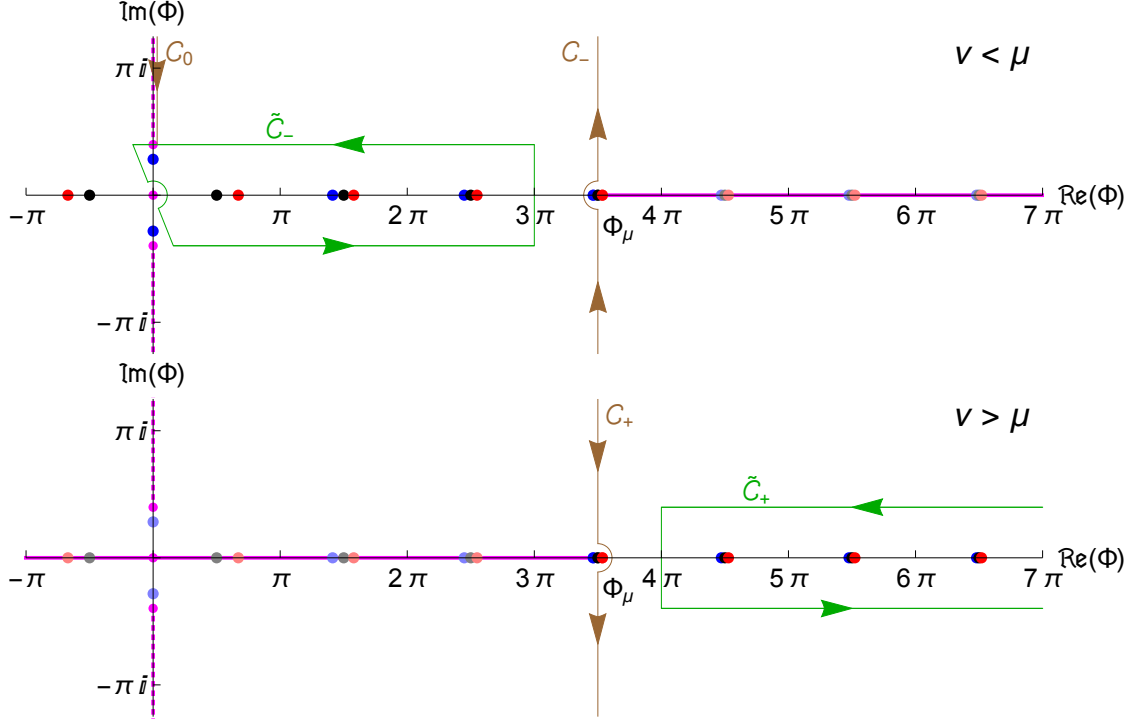


Figure 4. Complex zeroes of $P(\Phi)$ for three temperatures $x = \{-\frac{5}{4}, 0, \frac{5}{4}\}$ below (blue), at (black), and above (red) the critical point T_c , for $\mu = 4$. At $x = -1$ the first zero $\Phi_1 = 0$. The upper/lower plot shows the integration contours \tilde{C}_{\pm} from (41c) (green lines) as well as C_0 from (50) and C_{\pm} from (49) (brown lines) for the terms $\nu \leq \mu$, respectively. The log/sqrt branch cuts are shown as solid/dashed magenta lines.

B. Contour integration

We first calculate the regularized scaling limit \tilde{p}_{μ} of the product p_{μ} (I.74) using the rescaling

$$c_{\mu} - c_{\nu} = \cos \hat{\varphi}_{\mu} - \cos \hat{\varphi}_{\nu} \mapsto \cos \frac{\Phi_{\mu}}{M} - \cos \frac{\Phi_{\nu}}{M} = \frac{\Phi_{\nu}^2 - \Phi_{\mu}^2}{2M^2} + \mathcal{O}(M^{-4}). \quad (39)$$

An important simplification stems from the fact that the residual matrix \mathbf{Y} only contains products $p_{\mu \in \text{odd}} p_{\mu' \in \text{even}}$ of one odd and one even factor, respectively, such that μ -independent terms in $(\cdot)^{-\sigma_{\mu}\sigma_{\nu}}$ cancel in the resulting products. We can therefore drop the factor $1/2M^2$ and instead insert a regularizing denominator, that ensures the convergence of the infinite product, to get

$$\tilde{p}_{\mu} \equiv \lim_{N \rightarrow \infty} \frac{\prod'_{\nu=1}^N (\Phi_{\nu}^2 - \Phi_{\mu}^2)^{-\sigma_{\mu}\sigma_{\nu}}}{\prod_{\nu=1}^N (\Phi_{\nu}^2)^{-\sigma_{\mu}\sigma_{\nu}}} = \Phi_{\mu}^2 \prod'_{\nu=1}^{\infty} \left(1 - \frac{\Phi_{\mu}^2}{\Phi_{\nu}^2}\right)^{-\sigma_{\mu}\sigma_{\nu}}. \quad (40)$$

Here, \prod' denotes the regularized product, with zero and infinite factors removed. This alternating product over the zeroes Φ_ν of $P(\Phi)$ (33) can be calculated by complex contour integration using Cauchy's residue theorem: we first rewrite the product as two sums, split into terms $\nu < \mu$ and $\nu > \mu$, respectively, as we have to avoid the zero Φ_μ . In the first sum, the argument of the log is negated to always be positive, leading to an extra overall factor σ_μ . This circumvents the cut of the logarithm in the complex plane (solid magenta lines on the real axes in figure 4) in the resulting contour integrals. We find

$$\tilde{p}_\mu = \Phi_\mu^2 \exp \left[-\sigma_\mu \sum_{\nu=1}^{\infty}{}' \sigma_\nu \log \left(1 - \frac{\Phi_\mu^2}{\Phi_\nu^2} \right) \right] \quad (41a)$$

$$= \sigma_\mu \Phi_\mu^2 \exp \left[-\sigma_\mu \left\{ \sum_{\nu=1}^{\mu-1} \sigma_\nu \log \left(\frac{\Phi_\mu^2}{\Phi_\nu^2} - 1 \right) + \sum_{\nu=\mu+1}^{\infty} \sigma_\nu \log \left(1 - \frac{\Phi_\mu^2}{\Phi_\nu^2} \right) \right\} \right] \quad (41b)$$

$$= \sigma_\mu \Phi_\mu^2 \exp \left[-\sigma_\mu \sum_{\pm} \frac{1}{2\pi i} \oint_{\tilde{C}_\pm} d\Phi \log \left(\pm \frac{\Phi^2 - \Phi_\mu^2}{\Phi^2} \right) R(\Phi) \right], \quad (41c)$$

with alternating counting polynomial $R(\Phi)$ fulfilling

$$\text{Res}_{\Phi=\Phi_\nu} R(\Phi) = \sigma_\nu, \quad (42)$$

which will be constructed in the next chapter. The two contours \tilde{C}_\pm enclose the respective zeroes Φ_ν and are shown as green lines in figure 4.

C. Construction of counting polynomial $R(\Phi)$

The alternating counting polynomial $R(\Phi)$ satisfying (42) is constructed in the following way: we discriminate the even and odd zeroes by first rewriting⁵

$$P(\Phi) = \cos \Phi + \frac{x}{\Phi} \sin \Phi = \Re \left[e^{i\Phi} \left(1 + \frac{x}{i\Phi} \right) \right]. \quad (43)$$

Normalizing the modulus of $1 + x/(i\Phi)$ to one, the zeroes of the real part move to $\pm i$, and the condition for the odd (+) and even (-) zeroes becomes

$$P_\pm(\Phi) \equiv 1 \pm e^{i\Phi} \Gamma^{-1}(x + i\Phi) \stackrel{!}{=} 0, \quad (44)$$

with $\Gamma = \sqrt{x^2 + \Phi^2}$ from (36), leading to the odd and even counting polynomials

$$R_\pm(\Phi) \equiv Q'_\pm(\Phi), \quad (45)$$

⁵ The case $\mu = 1$, $x < -1$, with imaginary Φ_1 , has to be handled separately, but leads to the same result for P_\pm .

fulfilling $\text{Res}_{\Phi=\Phi_\nu} R_\pm(\Phi) = \delta_{\sigma_\nu, \pm 1}$, with symmetrized antiderivatives

$$Q_\pm(\Phi) \equiv \frac{1}{2} \log[P_\pm(\Phi)P_\pm(-\Phi)] = \frac{1}{2} \log \left[2 \left(1 \pm \frac{x}{\Gamma} \cos \Phi \mp \frac{\Phi}{\Gamma} \sin \Phi \right) \right]. \quad (46)$$

For the alternating counting polynomial $R(\Phi) \equiv Q'(\Phi)$ we find the antiderivatives

$$Q(\Phi) \equiv Q_+(\Phi) - Q_-(\Phi) = \text{artanh} \left(\frac{x}{\Gamma} \cos \Phi - \frac{\Phi}{\Gamma} \sin \Phi \right), \quad (47)$$

leading to the result

$$R(\Phi) = -\sqrt{\frac{\Gamma^2}{\Phi^2} \frac{1+x\Gamma^{-2}}{P(\Phi)}} \Big|_{\Phi \in \mathbb{C}^+} - \frac{\Gamma}{\Phi} \frac{1+x\Gamma^{-2}}{P(\Phi)} = \frac{-(x+x^2+\Phi^2)}{\sqrt{x^2+\Phi^2}(\Phi \cos \Phi + x \sin \Phi)}, \quad (48)$$

where \mathbb{C}^+ denotes the complex domain $\{z \in \mathbb{C} \mid -\frac{\pi}{2} < \arg z \leq \frac{\pi}{2} \vee z = 0\}$. The resulting analytic structure of the integrands is shown in figure 4. $R(\Phi)$ has square root branch cuts from $\pm ix$ to $\pm i\infty$ as well as a simple pole at zero, with residuum $\text{Res}_{\Phi=0} R(\Phi) = -1$. Additionally, the logarithm contributes log branch cuts running either from $-\Phi_\mu$ to Φ_μ for \mathcal{C}_+ , or from $\pm\Phi_\mu$ to $\pm\infty$ for \mathcal{C}_- .

D. Calculation of the integrals

We now deform the contour \tilde{C}_- to C_0 at the imaginary axis and to the line C_- and move \tilde{C}_+ to C_+ as shown in figure 4. The resulting contribution from C_\pm can be calculated using (47) and reads

$$-\sigma_\mu \sum_{\pm} \frac{1}{2\pi i} \int_{C_\pm} d\Phi \log \left(\pm \frac{\Phi^2 - \Phi_\mu^2}{\Phi^2} \right) R(\Phi) = -\log \left[\frac{\Phi_\mu}{4} (1+x\Gamma_\mu^{-2}) \right]. \quad (49)$$

The pole at zero and the special behavior of Φ_1 at $x = -1$ has to be carefully analyzed, leading to the result

$$\tilde{p}_\mu = \frac{4\sigma_\mu \Phi_\mu}{1+x\Gamma_\mu^{-2}} \left(\frac{x+1}{2x} \Phi_\mu \right)^{-\sigma_\mu} \exp \left[\frac{\sigma_\mu}{\pi i} \int_{|x|}^{i\infty} d\Phi \log \left(\left(\frac{x+1}{2x} \right)^{-2} \frac{\Phi_\mu^2 - \Phi^2}{\Phi^2 \Phi_\mu^2} \right) R(\Phi) \right], \quad (50)$$

where we have used the identity, c. f. (47),

$$\frac{1}{\pi i} \int_{|x|}^{i\infty} d\Phi R(\Phi) = \frac{1}{2} (\text{sign } x - 1). \quad (51)$$

In (50) we can again drop (μ -independent terms) $^{\sigma_\mu}$ to get

$$\tilde{p}_\mu^\dagger \equiv \frac{4\sigma_\mu \Phi_\mu^{1-\sigma_\mu}}{1+x\Gamma_\mu^{-2}} \exp \left[\frac{\sigma_\mu}{\pi i} \int_{|x|}^{i\infty} d\Phi \log \left(1 - \frac{\Phi^2}{\Phi_\mu^2} \right) R(\Phi) \right]. \quad (52)$$

We can combine this result for \tilde{p}_μ^\dagger with the scaling form of the coefficients \hat{v}_μ from (I.87a),

$$\hat{v}_\mu \mapsto \tilde{v}_\mu \equiv \tilde{p}_\mu^\dagger \sigma_\mu (\Gamma_\mu - \sigma_\mu x)^{\sigma_\mu} \quad (53)$$

to find, as $(\Gamma - x)(\Gamma + x) = \Phi^2$, the resulting scaling form of the matrix elements

$$\tilde{v}_\mu = 4 \frac{\Gamma_\mu - x}{1 + x\Gamma_\mu^{-2}} \exp \left[\frac{\sigma_\mu}{\pi i} \int_{|x|}^{i\infty} d\Phi \log \left(1 - \frac{\Phi^2}{\Phi_\mu^2} \right) R(\Phi) \right]. \quad (54a)$$

In the special case $\mu = 1$ at $x \rightarrow -1$, where $\Phi_1 \rightarrow 0$, the integral diverges logarithmically while the prefactor $\Gamma_\mu - x$ goes to zero. Using the series expansion around $x = -1$, $\Phi_1 = \sqrt{3(x+1)} + \mathcal{O}(x+1)^{3/2}$ we can nonetheless proceed and find

$$\tilde{v}_1|_{x=-1} = 12 \exp \left[\frac{1}{\pi i} \int_i^{i\infty} d\Phi \log(-\Phi^2) R(\Phi) \right] = 6.39303337215 \dots \quad (54b)$$

The scaling form of the Cauchy matrix \mathbf{T} from (I.70a) reads

$$(\tilde{\mathbf{T}})_{\mu\nu} \equiv \frac{1}{\Phi_\nu^2 - \Phi_\mu^2} = \frac{1}{\Gamma_\nu^2 - \Gamma_\mu^2}, \quad (55)$$

where we have moved the factor $2M^2$ from the expansion around $M = \infty$ into the Cauchy determinant (I.80). Combining (55) with the diagonal matrices

$$(\mathbf{\Gamma})_{\mu\mu} \equiv \Gamma_\mu, \quad (\tilde{\mathbf{V}})_{\mu\mu} \equiv \tilde{v}_\mu, \quad (56)$$

we find the result for the residual matrix \mathbf{Y} in the finite-size scaling limit

$$\tilde{\mathbf{Y}}(x, \rho) = -e^{-\rho\Gamma_e} \tilde{\mathbf{V}}_e \tilde{\mathbf{T}}_{e,o} e^{-\rho\Gamma_o} \tilde{\mathbf{V}}_o \tilde{\mathbf{T}}_{o,e}, \quad (57)$$

from which we can calculate the universal partition function scaling function Σ and the Casimir potential scaling function Ψ according to

$$\Sigma(x, \rho) = \det[\mathbf{1} + \tilde{\mathbf{Y}}(x, \rho)], \quad (58a)$$

$$\Psi(x, \rho) = -\rho^{-1} \log \Sigma(x, \rho). \quad (58b)$$

Note that Σ depends on the aspect ratio ρ only via the two exponentials in $\tilde{\mathbf{Y}}(x, \rho)$.

E. Representation of the partition function scaling function $\Sigma(x, \rho)$

While the scaled residual matrix $\tilde{\mathbf{Y}}$ is infinite dimensional, its matrix elements become exponentially small for large μ, ν at least if $\rho \gtrsim 1$,

$$(\tilde{\mathbf{Y}})_{\nu \in e, \mu \in o} = \mathcal{O}(e^{-\rho(\Gamma_1 + \Gamma_\nu)}), \quad (59)$$

such that we can take the upper left $N \times N$ submatrix for a rapidly converging calculation of the determinant. This direct approach is however only applicable for $N \lesssim 10$ if ρ is left as a free parameter, as the symbolic evaluation of a general $N \times N$ determinant is exponentially hard and requires $N!$ terms. However, we alternatively can expand the determinant according to (I.97) and directly calculate all terms $\mathcal{O}(e^{-2\pi\rho n})$ up to $n \leq N$. Therefore we define the set \mathcal{S}_n of all subsets \mathbf{s} of the natural numbers with equal number of even and odd elements μ fulfilling the condition

$$\mathcal{S}_n = \left\{ \mathbf{s} \mid \mathbf{s} \subset \mathbb{N} \wedge \sum_{\mu \in \mathbf{s}} \sigma_\mu = 0 \wedge \sum_{\mu \in \mathbf{s}} \left(\mu - \frac{1}{2}\right) = 2n \right\}, \quad (60)$$

e.g., $\mathcal{S}_1 = \{\{1, 2\}\}$ and $\mathcal{S}_4 = \{\{1, 8\}, \{3, 6\}, \{5, 4\}, \{7, 2\}, \{1, 3, 2, 4\}\}$. We then can define the N -th approximant to the partition function scaling function

$$\Sigma^{(N)}(x, \rho) \equiv 1 + \sum_{n=1}^N \sum_{\mathbf{s} \in \mathcal{S}_n} a_{\mathbf{s}} e^{-\rho \Gamma_{\mathbf{s}}}, \quad (61a)$$

with

$$a_{\mathbf{s}} \equiv \prod_{\{\mu, \nu\} \subset \mathbf{s}} (\Phi_\mu^2 - \Phi_\nu^2)^{-2\sigma_\mu \sigma_\nu} \prod_{\mu \in \mathbf{s}} \tilde{v}_\mu, \quad \Gamma_{\mathbf{s}} \equiv \text{Tr } \mathbf{\Gamma}_{\mathbf{s}} = \sum_{\mu \in \mathbf{s}} \Gamma_\mu, \quad (61b)$$

to get an exponentially precise approximation to the scaling function (58a)

$$\Sigma(x, \rho) = \Sigma^{(N)}(x, \rho) + o(e^{-2\pi\rho N}). \quad (62)$$

Note that (61a) is a perturbative series, and the number of elements in \mathcal{S}_n equals the famous integer partition function P_n from number theory [27], $|\mathcal{S}_n| = P_n$. Consequently, the calculation of, e.g., $\Sigma^{(30)}$ requires only 28629 terms instead of the $30! = 2.65 \times 10^{32}$ terms needed for the direct evaluation of the determinant.

In table II the leading coefficients $a_{\mathbf{s}}$ and $\Gamma_{\mathbf{s}}$ are given for the two cases $x = \pm 1$. Already with these few terms the error is smaller than $e^{-8\pi} \approx 10^{-11}$ for all $\rho \geq 1$, while the case $\rho < 1$ can be calculated using the symmetry under exchange of the two directions \updownarrow and \leftrightarrow [14, (52)],

$$\Theta(x, \rho) = \rho^{-2} \Theta(x\rho, \rho^{-1}). \quad (63)$$

With these expressions we now present results for the Casimir scaling functions. We first turn to the critical point $x = 0$.

order n	set \mathbf{s}	$x = -1$		$x = 1$	
		$a_{\mathbf{s}}$	$\Gamma_{\mathbf{s}}/2\pi$	$a_{\mathbf{s}}$	$\Gamma_{\mathbf{s}}/2\pi$
1	{1, 2}	0.41416034599	0.89179907560	0.15689480307	1.15797017264
2	{3, 2}	0.58023590813	1.97241431063	0.27677728168	2.07776833638
2	{1, 4}	0.02228040130	1.90188245064	0.01146254079	2.13146302530
3	{3, 4}	0.48130844027	2.98249768567	0.31674195444	3.05126118904
3	{5, 2}	0.05012321797	2.97699865033	0.02613926677	3.06476730850
3	{1, 6}	0.00537233691	2.90454040035	0.00297985504	3.12373747328
4	{5, 4}	0.47345042883	3.98708202537	0.34034540402	4.03826016115
4	{3, 6}	0.04512462939	3.98515563538	0.03206462405	4.04353563702
4	{7, 2}	0.01444309494	3.97874169683	0.00782432208	4.05964386240
4	{1, 8}	0.00206454953	3.90577401397	0.00118447481	4.12008924457
4	{1, 3, 2, 4}	0.31379568621	3.87429676127	0.07798039866	4.20923136168

Table II. Amplitudes $a_{\mathbf{s}}$ and exponents $\Gamma_{\mathbf{s}}$ from (61a) for $x = \pm 1$ and $n = 1, \dots, 4$.

V. RESULTS

A. Results at $x = 0$

At criticality $x = 0$ we work with the volume FSS functions Σ_{\circ} , Ψ_{\circ} and ψ_{\circ} in order to compare with conformal field theory (CFT) results. Remember that $\Sigma(0, \rho) = \Sigma_{\circ}(0, \rho)$, $\rho\Psi(0, \rho) = \Psi_{\circ}(0, \rho)$ and $\psi(0, \rho) = \psi_{\circ}(0, \rho)$. We use the superscript (0) for quantities at $x = 0$. For $x = 0$ the characteristic polynomial reduces to

$$P^{(0)}(\Phi) = \cos \Phi, \quad (64)$$

with trivial zeroes $\Phi_{\mu}^{(0)} = (\mu - \frac{1}{2})\pi$, $\mu \in \mathbb{N}$. Consequently, the infinite product $\tilde{p}_{\mu}^{\dagger}$ from (52) can be calculated exactly at $x = 0$ and can be expressed through the Euler beta function $B(a, b) = \Gamma(a)\Gamma(b)/\Gamma(a + b)$, with the result

$$\tilde{p}_{\mu}^{\dagger(0)} = 4\sigma_{\mu}\Phi_{\mu}^{(0)} \left[\frac{1}{\sqrt{2}\pi} B\left(\frac{\mu}{2}, \frac{1}{2}\right) \right]^{2\sigma_{\mu}}. \quad (65)$$

The resulting coefficients \tilde{v}_{μ} (54a) become

$$\tilde{v}_{\mu}^{(0)} = \tilde{p}_{\mu}^{\dagger(0)}\sigma_{\mu}(\Phi_{\mu}^{(0)})^{\sigma_{\mu}} = 4(\Phi_{\mu}^{(0)})^{1+\sigma_{\mu}} \left[\frac{1}{\sqrt{2}\pi} B\left(\frac{\mu}{2}, \frac{1}{2}\right) \right]^{2\sigma_{\mu}}, \quad (66)$$

and with

$$\tilde{\mathbf{Y}}(0, \rho) = -e^{-\rho\Phi_e^{(0)}} \tilde{\mathbf{V}}_e^{(0)} \tilde{\mathbf{T}}_{e,o}^{(0)} e^{-\rho\Phi_o^{(0)}} \tilde{\mathbf{V}}_o^{(0)} \tilde{\mathbf{T}}_{o,e}^{(0)} \quad (67)$$

from (57) and (58a) we arrive at the rapidly converging series

$$\Sigma_o(0, \rho) = 1 + \frac{1}{4}e^{-2\pi\rho} + \frac{13}{32}e^{-4\pi\rho} + \frac{55}{128}e^{-6\pi\rho} + \frac{1235}{2048}e^{-8\pi\rho} + \frac{4615}{8192}e^{-10\pi\rho} + \mathcal{O}(e^{-12\pi\rho}). \quad (68)$$

This result is identical to the prediction from conformal field theory [3], which can be written in several ways,

$$\Sigma_o(0, \rho) = e^{-\frac{\pi}{48}\rho} \eta^{-\frac{1}{4}}(i\rho) = (e^{-2\pi\rho})_\infty^{-\frac{1}{4}} = \Pi\left(-\frac{1}{4} \mid e^{-2\pi\rho}\right), \quad (69)$$

with the Dedekind eta function η , the q -Pochhammer symbol $(q)_\infty$, or in terms of the q -products introduced in (I.A2). Here we have taken into account the additional contribution $e^{-\frac{\pi}{48}\rho}$ from the strip geometry, see below for details. While we were not able to proof this correspondence, the series coefficients agree at least for the first 30 terms and we have no doubt about the equivalency.

Observing the fact that for both even and odd μ , $\tilde{v}_\mu^{(0)}$ is $2\pi^2$ times a squared rational number, we define the square root

$$\tilde{w}_\mu^{(0)} \equiv \sqrt{\tilde{v}_\mu^{(0)}} = 2 (\Phi_\mu^{(0)})^{\frac{1+\sigma_\mu}{2}} \left[\frac{1}{\sqrt{2\pi}} \text{B}\left(\frac{\mu}{2}, \frac{1}{2}\right) \right]^{\sigma_\mu} \quad (70a)$$

$$= \sqrt{2}\sigma_\mu \left(\mu - \frac{1}{2}\right)^{\frac{1+\sigma_\mu}{2}} \text{B}\left(\frac{1}{2} \left[\mu + \frac{1-\sigma_\mu}{2} \right], \frac{\sigma_\mu}{2}\right) \quad (70b)$$

as $\text{B}\left(\frac{\mu}{2}, \frac{1}{2}\right)^{-1} = -\frac{1}{2\pi} \text{B}\left(\frac{\mu+1}{2}, -\frac{1}{2}\right)$. The generating function $\mathcal{W}^{(0)}(\eta)$ of the coefficients $\tilde{w}_\mu^{(0)}$ can also be given and reads

$$\mathcal{W}^{(0)}(\eta) = \sum_{\mu=1}^{\infty} \tilde{w}_\mu^{(0)} \eta^{\mu-1} = \frac{\pi}{\sqrt{2}} \frac{1}{1-\eta} \sqrt{\frac{1+\eta}{1-\eta}}. \quad (71)$$

Using the coefficients $\tilde{w}_\mu^{(0)}$ we can write $\tilde{\mathbf{Y}}$ symmetrically: defining

$$\mathbf{X}(0, \rho) \equiv e^{-\frac{\rho}{2}\Phi_e^{(0)}} \tilde{\mathbf{W}}_e^{(0)} \tilde{\mathbf{T}}_{e,o}^{(0)} \tilde{\mathbf{W}}_o^{(0)} e^{-\frac{\rho}{2}\Phi_o^{(0)}} \quad (72)$$

we have

$$\Sigma_o(0, \rho) = \det\left(\mathbf{1} + \bar{\mathbf{X}}\mathbf{X}\right), \quad (73)$$

where the bar denotes the transpose. As a final remark, we point out that the general residual matrix (57) can also be written symmetrically using $\tilde{w} = \sqrt{\tilde{v}}$. However, \tilde{v} from

(54a) is not a formal square. Maybe this symmetric representation can be utilized to proof the equivalence of (68) and (69).

From (58b) and (68) the series of the strip Casimir potential scaling function $\Psi_{\circ}(0, \rho)$ reads, with $q \equiv e^{-2\pi\rho}$,

$$\Psi_{\circ}(0, \rho) = -\log \Sigma_{\circ}(0, \rho) \quad (74a)$$

$$= -\frac{1}{4} \left[q + \frac{3}{2}q^2 + \frac{4}{3}q^3 + \frac{7}{4}q^4 + \frac{6}{5}q^5 + \frac{12}{6}q^6 + \frac{8}{7}q^7 + \mathcal{O}(q^8) \right] \quad (74b)$$

$$= -\frac{1}{4} \sum_{n=1}^{\infty} \frac{\sigma(n)}{n} q^n, \quad (74c)$$

with the divisor sum function $\sigma(n) = \sum_{d|n} d$ [27].

The strip Casimir force at $x = 0$ is given by

$$\psi_{\circ}(0, \rho) = -\partial_{\rho} \Psi_{\circ}(0, \rho) = -\frac{\pi}{2} \sum_{n=1}^{\infty} \sigma(n) q^n = -\frac{\pi}{48} - \frac{i}{4} \frac{\eta'(i\rho)}{\eta(i\rho)} = \frac{\pi}{48} (E_2(i\rho) - 1), \quad (75a)$$

with Ramanujan's weight two Eisenstein series E_2 [28], and with special value at $\rho = 1$,

$$\psi_{\circ}(0, 1) = \frac{1}{16} - \frac{\pi}{48} = -0.0029498469 \dots \quad (75b)$$

All these results can easily be deduced from different representations of the double series

$$4\Psi_{\circ}(0, \rho) = -\sum_{j=1}^{\infty} \sum_{k=1}^{\infty} \frac{1}{k} q^{jk} = \sum_{j=1}^{\infty} \log(1 - q^j) = \log(q)_{\infty} = \frac{\pi\rho}{12} + \log \eta(i\rho) \quad (76)$$

which can be rewritten as a double sum over $n = jk$ and the divisors d of n ,

$$4\Psi_{\circ}(0, \rho) = -\sum_{n=1}^{\infty} \sum_{d|n} \frac{d}{n} q^n = -\sum_{n=1}^{\infty} \frac{\sigma(n)}{n} q^n. \quad (77)$$

The total Casimir force ϑ_{\circ} at $x_{\circ} = 0$ is even simpler than (75a) and reads

$$\vartheta_{\circ}(0, \rho) = \frac{\pi}{48} + \psi_{\circ}(0, \rho) = -\frac{i}{4} \frac{\eta'(i\rho)}{\eta(i\rho)} = \frac{\pi}{48} E_2(i\rho), \quad (78)$$

leading to the result of Cardy & Peschel [2], that the amplitude of the logarithmic divergence of the Ising finite size free energy is $\frac{1}{16}$, as

$$\vartheta_{\circ}(0, 1) = \frac{\pi}{48} + \left(\frac{1}{16} - \frac{\pi}{48} \right) = \frac{1}{16}. \quad (79)$$

In chapter VD we will return to this point.

B. Results for general x and ρ

Using (61), we can calculate the FSS functions for given x with arbitrary precision, while the aspect ratio ρ remains a free parameter in the expressions. However, we first have to estimate the surface-corner contribution $\Theta_{s,c}(x)$ for a complete picture.

C. The Casimir potential scaling function $\Theta(x, \rho)$

For the computation of the (total) Casimir potential scaling function $\Theta(x, \rho)$ we need the surface-corner contribution $\Theta_{s,c}(x)$ from (19),

$$\Theta_{s,c}(x) = -\rho\Theta^{(oo)}(x) + \log \Sigma(x, \rho) + \Theta_o(x_o, \rho) \quad \forall \rho, \quad (80)$$

with volume scaling variable $x_o = x\rho^{1/2}$ from (13), that unfortunately could not be calculated directly from the regularized FSS limit of $F_{s,c}^{\text{res}}(L_\uparrow)$ yet. However, we can utilize the symmetry of the square, where $\rho = 1$, under the exchange of the two lattice directions \leftrightarrow and \updownarrow , which implies $\partial_\rho\Theta_o(x_o, \rho)|_{\rho=1} = 0$ [14], together with (18b), (16) and the $2d$ Ising value $d\nu = 2$. We get the scaling relation

$$\vartheta_o(x_o, 1) = -\frac{x_o}{2} \frac{\partial}{\partial x_o} \Theta_o(x_o, 1), \quad (81)$$

which can be solved for $\Theta_o(x_o, 1)$ to find, using (26),

$$\Theta_o(x_o, 1) = 2 \int_{x_o}^{x_o\infty} d\xi \xi^{-1} \vartheta_o(\xi, 1) \quad (82a)$$

$$= \underbrace{-2 \int_{x_o}^{x_o\infty} d\xi \xi^{-1} \Theta^{(oo)}(\xi)}_{I_o^{(1)}(x_o)} + \underbrace{2 \int_{x_o}^{x_o\infty} d\xi \xi^{-1} \psi_o(\xi, 1)}_{I_o^{(2)}(x_o)}. \quad (82b)$$

As $\vartheta_o(0, 1) = \frac{1}{16}$, $\Theta^{(oo)}(0) = -\frac{\pi}{48}$ and $\psi_o(0, 1) = \frac{1}{16} - \frac{\pi}{48}$ are all finite, see last chapter, the integrals $I_o^{(1,2)}(x_o)$, and consequently $\Theta_o(x_o, 1)$, diverge logarithmically at $x_o = 0$.

The integral $I_o^{(1)}(x_o)$ over $\Theta^{(oo)}$ from (21) can be evaluated analytically by exchanging the two integrals and using the formula $\int_x^\infty d\xi \log(1 + ae^{-b\xi}) = -b^{-1}\text{Li}_2(-ae^{-bx})$, with polylogarithm Li , with the result

$$I_o^{(1)}(x_o) = -\frac{1}{2\pi} \int_{|x_o|}^\infty d\Omega \frac{1}{\sqrt{\Omega^2 - x_o^2}} \text{Li}_2\left(-\frac{\Omega - x_o}{\Omega + x_o} e^{-2\Omega}\right). \quad (83a)$$

To leading order, $I_{\circ}^{(1)}$ diverges logarithmically and has a jump at zero from the change of the integration limits,

$$I_{\circ}^{(1)}(x_{\circ}) \simeq -\frac{\pi}{24} \log |x_{\circ}| - C \frac{|x_{\circ}|}{x_{\circ}}, \quad (83b)$$

with Catalan's constant C .

The second integral $I_{\circ}^{(2)}(x_{\circ})$ has to be evaluated numerically, so we split off the log singularity and write

$$I_{\circ}^{(2)}(x_{\circ}) = \psi_{\circ}(0, 1) \log(1 + x_{\circ}^{-2}) + 2 \int_{x_{\circ}}^{x_{\circ}\infty} d\xi \xi^{-1} \left[\psi_{\circ}(\xi, 1) - \frac{1}{1 + \xi^2} \psi_{\circ}(0, 1) \right]. \quad (84a)$$

While the integrand is analytic at $x_{\circ} = 0$, the integral again develops a jump discontinuity at $x_{\circ} = 0$ from the different integration limits above and below zero,

$$I_{\circ}^{(2)}(x_{\circ}) \simeq -\left(\frac{1}{8} - \frac{\pi}{24}\right) \log |x_{\circ}| + \left(C - \frac{3}{4} \log 2\right) \frac{|x_{\circ}|}{x_{\circ}}. \quad (84b)$$

Via the low-temperature integration limit in (84a) we have respected the additional contribution $-\log 2$ due to the broken symmetry in the ordered phase, see [14] for details, that was inadvertently attributed to the corner free energy $f_c^<$ in [1, 4]. Therefore, $\Theta_{s,c}(x \rightarrow -\infty) = \Theta_{\circ}(x_{\circ} \rightarrow -\infty, \rho) = -\log 2$ in agreement with the corner-free toroidal and cylindrical case [14, 15], while $f_c \rightarrow 0$ both in the high- and low-temperature limit.

As both $\Theta^{(\circ\circ)}(x)$ and $\log \Sigma(x, \rho)$ are analytic around $x = 0$, $\Theta_{s,c}(x)$ from (80) fulfills

$$\Theta_{s,c}(x) = -\frac{1}{8} \log |x| - \frac{3}{4} \log 2 \frac{|x|}{x} + \text{regular terms} \quad (85)$$

for small x . The same asymptotic behavior holds for the Casimir potential, but with a different (in)dependency on ρ ,

$$\Theta_{\circ}(x_{\circ}, \rho) = -\frac{1}{8} \log |x_{\circ}| - \frac{3}{4} \log 2 \frac{|x_{\circ}|}{x_{\circ}} + \text{terms regular in } x_{\circ}. \quad (86)$$

Remember that Θ_{\circ} is a function symmetric under $\leftrightarrow / \updownarrow$ exchange, while $\Theta_{s,c}$ is a property of the \leftrightarrow boundary. The result for $\Theta_{s,c}(x)$ is shown in figure 5, together with the Casimir potential scaling function $\Theta(x, \rho)$ for several values of $\rho \geq 1$. The behavior of both quantities is dominated by the logarithmic divergence at $x = 0$. Furthermore, both are much larger below criticality, which is expected for systems with open boundary conditions.

While the (total) Casimir potential $\Theta(x, \rho)$ diverges logarithmically for $x \rightarrow 0$ and therefore is infinite at criticality for all finite aspect ratios $0 < \rho < \infty$, we can nevertheless

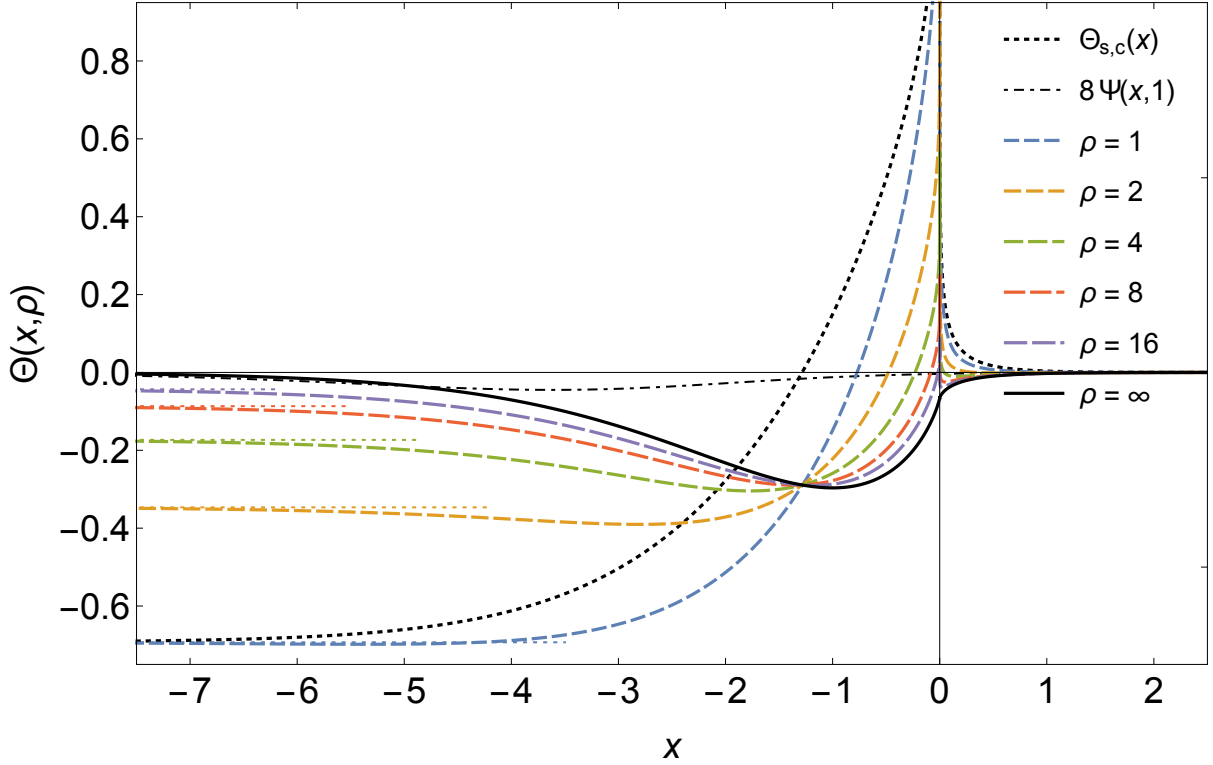


Figure 5. Universal Casimir potential scaling function $\Theta(x, \rho)$ for the Ising rectangle with different aspect ratios $\rho \geq 1$, together with the surface-corner contribution $\Theta_{s,c}(x)$ and the strip residual contribution $\Psi(x, 1)$. The latter is multiplied by 8. The corresponding curves for $\rho < 0$ fulfill (63). Note that $\Theta(x \rightarrow -\infty, \rho) = -\rho^{-1} \log 2$ (dotted lines).

subtract the divergent contribution $\Theta_{s,c}(x)$ and define a finite Casimir amplitude

$$\Delta_{\circ}(\rho) \equiv \lim_{x \rightarrow 0} [\rho \Theta(x, \rho) - \Theta_{s,c}(x)] = \rho \Theta^{(\infty)}(0) + \Psi_{\circ}(0, \rho) = \frac{1}{4} \log \eta(i\rho). \quad (87)$$

As consequence, we have the unusual situation that the (finite) Casimir amplitude is different from the (divergent) Casimir potential at criticality.

In summary, we observe the following logarithmic contributions to the total free energy F and its residual F_{∞}^{res} : the total finite-size free energy (1) has a log term at criticality, originally predicted by Cardy & Peschel [2] using conformal field theory,

$$F(\tau=0; L, M) = LM f_b(0) + [L + M] f_s(0) - \frac{1}{16} \log(LM) + \text{regular terms}, \quad (88a)$$

with reduced temperature $\tau = 1 - z/z_c$, while the infinite volume contribution (3b) has log

terms and a jump originating from the corner free energy, see (B1) in the appendix,

$$F_\infty(\tau; L, M) = LM f_b(\tau) + [L + M] f_s(\tau) + \frac{1}{8} \log |\tau| + \frac{3}{4} \log 2 \frac{|\tau|}{\tau} + \text{regular terms} \quad (88b)$$

such that

$$F_\infty^{\text{res}}(\tau; L, M) = -\frac{1}{16} \log(\tau^2 LM) - \frac{3}{4} \log 2 \frac{|\tau|}{\tau} + \text{regular terms}. \quad (88c)$$

In the FSS limit, where $x_\circ = 2\tau\sqrt{LM}$ and $\rho = L/M$, both log contributions combine to (86). We conclude that both the logarithmic divergence and the jump in the Casimir potential scaling function $\Theta_\circ(x_\circ, \rho)$ (86) stem from the near critical behavior of the corner free energy f_c .

D. The Casimir force scaling function $\vartheta(x, \rho)$

Finally we come to the Casimir force scaling function $\vartheta(x, \rho)$ at arbitrary x and ρ . From (26) we can easily determine the Casimir force with high precision, provided $\rho \gtrsim 1$,

$$\vartheta(x, \rho) = -\Theta^{(\circ\circ)}(x) + \psi(x, \rho). \quad (89)$$

For $\rho \lesssim 1$, however, the convergence is suboptimal, and we instead use (18a) and the $\leftrightarrow, \updownarrow$ exchange symmetry and calculate the Casimir force in \updownarrow direction instead, to get the equivalent expression

$$\vartheta(x, \rho) = \vartheta^{(\circ\circ)}(x) - \rho x \Theta'_{s,c}(x) - \frac{x \partial}{\partial x} \Psi(x, \rho^{-1}) - \psi(x, \rho^{-1}), \quad (90)$$

with [24–26]

$$\vartheta^{(\circ\circ)}(x) \equiv -\frac{1}{\pi} \int_0^\infty d\omega \sqrt{x^2 + \omega^2} \left(1 + \frac{\sqrt{x^2 + \omega^2} + x}{\sqrt{x^2 + \omega^2} - x} e^{2\sqrt{x^2 + \omega^2}} \right)^{-1} \quad (91)$$

from (18a), that does not suffer from convergence problems if $\rho \lesssim 1$. At $\rho = 1$ we can derive the expression

$$x \Theta'_{s,c}(x) = \Theta^{(\circ\circ)}(x) + \vartheta^{(\circ\circ)}(x) - 2\psi(x, 1) - \frac{x \partial}{\partial x} \Psi(x, 1), \quad (92)$$

that implies that $-x \Theta'_{s,c}(x)$ is approximately equal to the difference $\vartheta_{\updownarrow}(x_{\updownarrow}, \infty) - \vartheta_{\leftrightarrow}(x_{\leftrightarrow}, 0)$, that is, the distance between the dashed and the solid black curves in figure 6.

The resulting universal Casimir force scaling functions for different values of the aspect ratio ρ are displayed in figure 6. The force is attractive for small aspect ratios $\rho \lesssim 1/4$

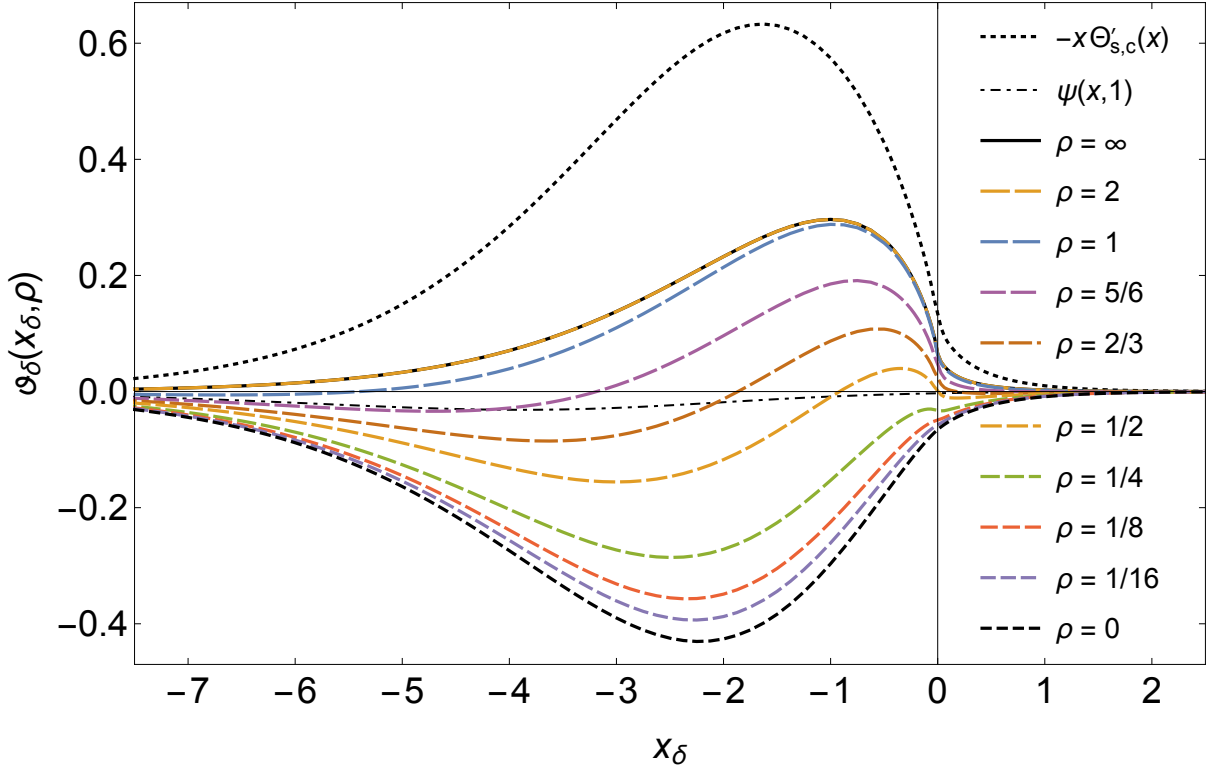


Figure 6. Universal Casimir force scaling function $\vartheta_\delta(x_\delta, \rho)$ for the Ising rectangle with different aspect ratios ρ . For $\rho \geq 1$ we show $\vartheta \equiv \vartheta_\uparrow$ over $x \equiv x_\uparrow$ as defined by (18c), while for $\rho \leq 1$ we show $\vartheta_{\leftrightarrow}$ over x_{\leftrightarrow} from (18a). Note that the curve for $\rho = \infty$ is masked behind the curve for $\rho = 2$. Also shown are the surface-corner contribution $-x\Theta'_{s,c}(x)$ from (92) and the strip contribution $\psi(x, 1)$ from (28) to the Casimir force.

and becomes repulsive for larger aspect ratios, a behavior which is very similar to the fully periodic case [14, 15]. However, the force at criticality $x = 0$ in a square system $\rho = 1$ does not vanish such as in the periodic case. This is directly related to the log divergence of the corresponding Casimir potential and is interpreted as a consequence of a long-range repulsive corner-corner interaction. At criticality, the Casimir force changes sign at $\rho_0 = 0.523521700017999266800\dots$ and is attractive for $\rho < \rho_0$. Note that $i\rho_0$ is the only purely imaginary zero of the Eisenstein series E_2 .

VI. SCALING LIMIT OF EFFECTIVE SPIN MODEL

Finally, we discuss the FSS limit of the effective spin model introduced in (I.99). In the FSS limit $M \rightarrow \infty$, $T \rightarrow T_c$ with constant x and ρ , we find the thermodynamic limit $N \rightarrow \infty$ of the scaled reduced Hamiltonian

$$\tilde{\mathcal{H}}_{\text{eff}}(x, \rho) = - \sum_{\mu < \nu = 1}^N \tilde{K}_{\mu\nu}(x) s_\mu s_\nu + \rho \sum_{\mu=1}^N \Gamma_\mu(x) s_\mu + b \left[\sum_{\mu=1}^N \sigma_\mu s_\mu \right]^2, \quad (93)$$

with scaled interaction constants

$$\tilde{K}_{\mu\nu} = -\sigma_\mu \sigma_\nu \log \frac{\tilde{v}_\mu \tilde{v}_\nu}{(\Phi_\mu^2 - \Phi_\nu^2)^2}, \quad (94)$$

and with \tilde{v}_μ from (54a).

For large $\mu + \nu$, with $\nu - \mu \ll \nu + \mu$, the interactions are asymptotically

$$\tilde{K}_{\mu\nu} \simeq 2\sigma_\mu \sigma_\nu \log \left[\frac{\pi}{2} |\nu - \mu| \right], \quad (95)$$

while for large ν with $\mu \ll \nu$

$$\tilde{K}_{\mu\nu} = 2\sigma_\mu \sigma_\nu \log \left[\frac{\pi^{3/2} \nu^{3/2}}{2^{3/2} (\mu - \frac{1}{2}) \text{B}(\frac{\mu}{2}, \frac{1}{2})} [1 + \mathcal{O}(\nu^{-1})] \right]. \quad (96)$$

In all cases the interaction grows logarithmically with μ and ν .

The aspect ratio ρ takes the role of an applied homogeneous magnetic field, which acts on the spins $s_\mu \in \{0, 1\}$ via a magnetic moment Γ_μ that grows linearly with μ . As a consequence, the spins are asymptotically fixed to $s_\mu = 0$ for large μ if $\rho > 0$, such that the spin dynamics is mainly restricted to the first few spins.

The strip Casimir force scaling function is related to the magnetization scaling function of the effective model, c.f. (I.103),

$$\psi(x, \rho) = \frac{\partial}{\partial \rho} \log \Sigma(x, \rho) = - \left\langle \sum_{\mu=1}^{\infty} \Gamma_\mu s_\mu \right\rangle_{\text{eff}} = - \sum_{\mu=1}^{\infty} \Gamma_\mu \langle s_\mu \rangle_{\text{eff}} = -\tilde{M}_{\text{eff}}(x, \rho). \quad (97)$$

To summarize, we can define a universal effective spin model (93) describing the FSS limit of the $2d$ Ising model on the rectangle. The couplings $\tilde{K}_{\mu\nu}$ between the spins as well as the magnetic moments Γ_μ depend on x , while the aspect ratio ρ takes the role of a homogeneous magnetic field. Thermodynamic quantities of this model are directly related to universal scaling functions of the underlying Ising universality class.

VII. CONCLUSIONS

Based on the results published recently [1], we calculated the universal finite-size scaling functions of the Casimir potential and the Casimir force for the Ising universality class on the $L \times M$ rectangle, with open boundary conditions in both directions, and with arbitrary aspect ratio ρ . The calculations were done in the finite-size scaling limit $L, M \rightarrow \infty, T \rightarrow T_c$, with fixed temperature scaling variable $x \propto (T/T_c - 1)M$ and fixed aspect ratio $\rho \propto L/M$. We have analytically derived exponentially fast converging series for the related Casimir potential and Casimir force scaling functions. At the critical point $T = T_c$ we could confirm predictions from conformal field theory for both the size dependent critical free energy (88a) [2] as well as for the shape dependence of the Casimir amplitude $\Delta_\circ(\rho)$ (87) [3].

The presence of corners and the related corner free energy has dramatic impact on the Casimir scaling functions and leads to a logarithmic divergence of the Casimir potential scaling function at criticality. As consequence, we have the unusual situation that the (finite) Casimir amplitude is different from the (divergent) Casimir potential at criticality. This behavior was not known from other geometries and boundary conditions.

These strong influence of system corners on the critical Casimir force might give rise to new applications in the framework of colloidal suspensions confined in finite near-critical binary liquid mixtures [29, 30].

ACKNOWLEDGMENTS

The author thanks Hendrik Hobrecht, Felix M. Schmidt and Jesper L. Jacobsen for helpful discussions and inspirations. I also thank my wife Kristine for her great patience during the preparation of this manuscript. This work was partially supported by the Deutsche Forschungsgemeinschaft through Grant HU 2303/1-1.

Appendix A: Series expansion for zeroes Φ_μ

We derive a series representation of Φ_μ in terms of the values $\Phi_\mu^{(0)}$ at $x = 0$ around $\Phi_\mu^{(0)} = \infty$: writing $\Phi_{0,\mu} \equiv \Phi_\mu^{(0)}$ and with

$$\Phi_\mu = \Phi_{0,\mu} + \Delta_\mu \tag{A1}$$

we have

$$P(\Phi_\mu) = P(\Phi_{0,\mu} + \Delta_\mu) = \frac{x}{\Phi_{0,\mu} + \Delta_\mu} \cos \Delta_\mu - \sin \Delta_\mu = 0, \quad (\text{A2})$$

leading to the recursion relation

$$\Delta_\mu^{(k)} \mapsto \Delta_\mu^{(k+1)} = \arctan \left(\frac{x}{\Phi_{0,\mu} + \Delta_\mu^{(k)}} \right). \quad (\text{A3})$$

This recursion can easily be performed analytically with a computer algebra system like *Mathematica* [31]: Starting with an empty series expansion $\Delta_\mu^{(0)} = \mathcal{O}(\Phi_{0,\mu}^{-1})$, we can simply apply (A3) n times using the command

$$\Delta_\mu[\mathbf{n}_-] := \text{Nest} \left[\text{ArcTan} \left[\frac{x}{\Phi_{0,\mu} + \#} \right] \&, \text{Series} \left[\frac{1}{\Phi_{0,\mu}}, \{\Phi_{0,\mu}, \infty, 0\} \right], \mathbf{n} \right] \quad (\text{A4})$$

to get the correct series expansion up to $\mathcal{O}(\Phi_{0,\mu}^{-(2n+1)})$, with the result

$$\Phi_\mu^2 = \Phi_{0,\mu}^2 + 2x - \frac{x^2(2x+3)}{3\Phi_{0,\mu}^2} + \frac{2x^3(x^2+5x+5)}{5\Phi_{0,\mu}^4} + \mathcal{O}(\Phi_{0,\mu}^{-6}) \quad (\text{A5})$$

for Φ_μ^2 .

Appendix B: Expansion of q -products around $q = 1$

The isotropic corner free energy near T_c can be derived from the q -product representation of Vernier & Jacobsen [8] as well as from (I.A7d). Written in terms of the reduced temperature $\tau = 1 - z/z_c$, the expansion is given by

$$f_c(\tau) = \frac{1}{8} \log |\tau| - \frac{2}{\pi} C + \frac{9}{16} \log 2 + \frac{3}{4} \log 2 \frac{|\tau|}{\tau} + \mathcal{O}(\tau), \quad (\text{B1})$$

with Catalan's constant C .

The isotropic surface free energy near T_c is calculated using the result of McCoy & Wu [7, (4.35)] together with an expansion of the q -products derived in [8] and (I.A7) to be

$$f_s(\tau) = f_s(0) + \frac{|\tau|}{2} + \left(\frac{1}{4} - \frac{3 \log 2}{2\pi} + \frac{\log |\tau| - 1}{\pi} \right) \tau + \mathcal{O}(\tau^2). \quad (\text{B2})$$

The critical value reads

$$\begin{aligned} f_s(0) &= -\frac{3}{4} \log z_c - 2 \left[\zeta^{(1,0)}\left(-1, \frac{1}{8}\right) + \zeta^{(1,0)}\left(-1, \frac{3}{8}\right) - \zeta^{(1,0)}\left(-1, \frac{5}{8}\right) - \zeta^{(1,0)}\left(-1, \frac{7}{8}\right) \right] \\ &= 0.1817314169844 \dots, \end{aligned} \quad (\text{B3})$$

with generalized Riemann zeta function $\zeta(s, a) = \sum_{k=0}^{\infty} (k+a)^{-s}$. Note that the exact value of the critical surface free energy $f_s(0)$ given in (B3) was not published yet. Both (B1) and (B3) can be derived from the product representations (I.A5b) and (I.A7b), expanded around the limit $q \rightarrow 1$.

-
- [1] Alfred Hucht. The square lattice Ising model on the rectangle I: finite systems. *J. Phys. A: Math. Theor.*, 50(6):065201, 2017. arXiv:1609.01963.
 - [2] John Cardy and Ingo Peschel. Finite-size dependence of the free energy in two-dimensional critical systems. *Nucl. Phys. B*, 300:377, 1988.
 - [3] P Kleban and I Vassileva. Free energy of rectangular domains at criticality. *J. Phys. A: Math. Gen.*, 24:3407, 1991.
 - [4] R. J. Baxter. The bulk, surface and corner free energies of the square lattice Ising model. *J. Phys. A: Math. Theor.*, 50(1):014001, 2017. arXiv:1606.02029.
 - [5] M. E. Fisher and P.-G. de Gennes. Phénomènes aux parois dans un mélange binaire critique. *C. R. Acad. Sci. Paris, Ser. B*, 287:207, 1978.
 - [6] L. Onsager. Crystal statistics. I. A two-dimensional model with an order-disorder transition. *Phys. Rev.*, 65:117, 1944.
 - [7] B. M. McCoy and T. T. Wu. *The Two-Dimensional Ising Model*. Harvard University Press, Cambridge, 1973.
 - [8] Eric Vernier and Jesper Lykke Jacobsen. Corner free energies and boundary effects for Ising, Potts and fully-packed loop models on the square and triangular lattices. *J. Phys. A: Math. Theor.*, 45:045003, 2012. arXiv:1110.2158.
 - [9] H. W. Diehl, Daniel Grüneberg, Martin Hasenbusch, Alfred Hucht, Sergei B. Rutkevich, and Felix M. Schmidt. Exact thermodynamic Casimir forces for an interacting three-dimensional model system in film geometry with free surfaces. *EPL*, 100(1):10004, Oct 2012. arXiv:1205.6613.
 - [10] H. W. Diehl, Daniel Grüneberg, Martin Hasenbusch, Alfred Hucht, Sergei B. Rutkevich, and Felix M. Schmidt. Large- n approach to thermodynamic Casimir effects in slabs with free surfaces. *Phys. Rev. E*, 89:062123, Jun 2014. arXiv:1402.3510.
 - [11] Alfred Hucht. On the symmetry of universal finite-size scaling functions in anisotropic systems.

- J. Phys. A: Math. Gen.*, 35:L481, Aug 2002.
- [12] D. P. Landau and R. H. Swendsen. Monte Carlo renormalization-group study of the rectangular Ising ferromagnet: Universality and a fixed line. *Phys. Rev. B*, 30:2787, 1984.
- [13] J. O. Indekeu, M. P. Nightingale, and W. V. Wang. Finite-size interaction amplitudes and their universality: Exact, mean-field, and renormalization-group results. *Phys. Rev. B*, 34(1):330–342, Jul 1986.
- [14] Alfred Hucht, Daniel Grüneberg, and Felix M. Schmidt. Aspect-ratio dependence of thermodynamic Casimir forces. *Phys. Rev. E*, 83:051101, Mar 2011.
- [15] Hendrik Hobrecht and Alfred Hucht. Critical Casimir force scaling functions of the two-dimensional Ising model at finite aspect ratios. *J. Stat. Mech.: Theory Exp.*, 2017:024002, Feb 2017. arXiv:1611.05622.
- [16] Alfred Hucht. Thermodynamic Casimir effect in ^4He films near T_λ : Monte Carlo results. *Phys. Rev. Lett.*, 99(18):185301, Nov 2007.
- [17] R. Garcia and M. H. W. Chan. Critical fluctuation-induced thinning of ^4He films near the superfluid transition. *Phys. Rev. Lett.*, 83:1187, 1999.
- [18] O. Vasilyev, A. Gambassi, A. Maciołek, and S. Dietrich. Monte Carlo simulation results for critical Casimir forces. *EPL*, 80:60009, 2007.
- [19] O. Vasilyev, A. Gambassi, A. Maciołek, and S. Dietrich. Universal scaling functions of critical Casimir forces obtained by Monte Carlo simulations. *Phys. Rev. E*, 79(4):041142, 2009.
- [20] M. Fukuto, Y. F. Yano, and P. S. Pershan. Critical Casimir effect in three-dimensional Ising systems: Measurements on binary wetting films. *Phys. Rev. Lett.*, 94:135702, 2005.
- [21] C. Hertlein, L. Helden, A. Gambassi, S. Dietrich, and C. Bechinger. Direct measurement of critical Casimir forces. *Nature*, 451:172, 2008.
- [22] A. Gambassi, A. Maciołek, C. Hertlein, U. Nellen, L. Helden, C. Bechinger, and S. Dietrich. Critical Casimir effect in classical binary liquid mixtures. *Phys. Rev. E*, 80(6):061143, Dec 2009.
- [23] Andrea Gambassi. The Casimir effect: From quantum to critical fluctuations. *Journal of Physics: Conference Series*, 161(1):012037, 2009.
- [24] Helen Au-Yang and Michael E. Fisher. Wall effects in critical systems: Scaling in Ising model strips. *Phys. Rev. B*, 21:3956, 1980.
- [25] R. Evans and J. Stecki. Solvation force in two-dimensional Ising strips. *Phys. Rev. B*, 49:8842–

8851, Apr 1994.

- [26] J. G. Brankov, D. M. Dantchev, and N. S. Tonchev. *Theory of Critical Phenomena in Finite-Size Systems – Scaling and Quantum Effects*. World Scientific, Singapore, 2000.
- [27] G. H. Hardy and E. M. Wright. *An Introduction to the Theory of Numbers*. Oxford Univ. Press, Oxford, 5 edition, 1979.
- [28] Eric W. Weisstein. *Eisenstein Series*. From MathWorld—A Wolfram Web Resource. <http://mathworld.wolfram.com/EisensteinSeries.html>.
- [29] Hendrik Hobeucht and Alfred Hucht. Direct simulation of critical Casimir forces. *EPL*, 106(5):56005, Jun 2014. arXiv:1405.4088.
- [30] Hendrik Hobeucht and Alfred Hucht. Many-body critical Casimir interactions in colloidal suspensions. *Phys. Rev. E*, 92:042315, Oct 2015.
- [31] Wolfram Research, Inc. *Mathematica V11.0*. Champaign, Illinois, 2016.